# Effect of microbubble-induced cavitation on the dispersion of sprays

D. D. van der Voort,[1,*] N. J. Dam,[2] R. P. J. Kunnen,[1] G. J. F. van Heijst,[1] and H. J. H. Clercx[1]
[1]*J.M. Burgerscenter for Fluid Dynamics & Turbulence and Vortex Dynamics, Applied Physics Department, Eindhoven University of Technology, 5612 AZ Eindhoven, The Netherlands*
[2]*Mechanical Engineering Department, Eindhoven University of Technology, 5612 AZ Eindhoven, The Netherlands*
(Received 30 June 2016; published 20 March 2017)

The presence of bubbles and voids inside nozzles has a large effect on the morphology and atomization of sprays. In this investigation the voids formed by microbubbles entering the nozzle are investigated using transparent glass nozzles, pressure transducers, and high-speed diffuse backlight imaging. A correlation is found between the magnitude of pressure pulses inside the nozzle and the size of the bubbles causing these pulses. This relation allows the prediction of cavity formation also in nontransparent nozzles, which allow more realistic conditions of operation. Subsequently, the direct measurements of dispersion derived from the spread of glowing fluid showed no significant increase of the dispersion compared to cavitation-free conditions. This indicates that, while the spray angle may increase, the turbulence (in both liquid and gas phase) that governs the dispersion remains the same and the cavitation bubble events do not have a significant impact on this process.

DOI: 10.1103/PhysRevFluids.2.033601

## I. INTRODUCTION

The breakup of sprays is governed by complex physical phenomena. It is a combination of turbulence, entrainment, evaporation, and cavitation that determines the spray morphology and evaporation during the breakup process. Understanding the atomization and dispersion of sprays has been a priority in fields such as diesel spray combustion and spray drying [1–4]. This dispersion is governed by the breakup process of the fluid as it exits the nozzle. Understanding the influence of each individual phenomenon on the whole is of paramount importance in predictions and optimization of spray breakup and the resulting droplet size distributions. Cavitation, the formation of vapor bubbles or voids in the nozzle capillary, has a distinct influence on the morphology of sprays [5–8]. While the influence of cavitation on mass flow and spray widths has been investigated for decades, the contribution of cavitation on the dispersion during breakup, the spread of fluid as it exits the nozzle, is still unknown.

An increase in spray angle, a qualitative indicator of spray width, was observed related to the presence of cavitation bubbles [5], as well as an asymmetry arising from the position of the vapor layer along the nozzle boundary [6]. The void in the nozzle capillary allows instabilities to form in the liquid-vapor boundary layer due to shear-induced turbulence. Furthermore, the free surface generated at the void will locally increase fluid velocity, further increasing the shear-induced turbulence. If the vapor layer collapses before it reaches the nozzle exit, the pressure fluctuations induced by the implosion may also have an effect on the ligament formation [9]. This indicates that the atomization and dispersion of the spray may be altered by the presence of a cavity. However, investigating the quantitative effect on the dispersion requires the ability to detect when cavities form inside the nozzle, as well as a measure of the size of these cavities.

There are several methods to detect the formation of cavities in nozzle capillaries. Transparent glass nozzles can be used to visualize bubbles and voids using diffuse backlight illumination (DBI) techniques [9–11]. This technique allows visualization of both the spray and the internal nozzle

*d.d.v.d.voort@tue.nl

 

liquid at the same time, with liquid transparent and gas dark inside the nozzle (due to refractive index changes) and the spray dark outside the nozzle (due to its high optical density). However, this only works for transparent nozzles. Glass nozzles are less relevant from an application point of view due to a limited injection pressure and more importantly the low roughness of the wall. The smooth wall reduces the generation of turbulence inside the nozzle capillary, removing the perturbations that initiate the breakup of the spray. X-ray imaging can be used to visualize internal density differences inside nontransparent (steel) nozzles and is able to detect cavities even at industrial (engine) conditions [12,13]. However, this does require access to a source of high-energy x-rays. The limited repetition rate of many such sources also requires the investigated flow to be statistically invariant. These studies have only investigated the flow under steadily cavitating conditions, caused by large pressure drops over the nozzle capillary. To investigate the influence of cavitation on spray breakup in a quantitative sense, both noncavitating and cavitating flow must be able to occur under the same experimental conditions. In the current study, microbubbles will be seeded upstream of the nozzle capillary to create unsteady cavitation bubbles to mimic cavitation phenomena. There is a difference in density and viscosity of the nitrogen gas bubbles and that of vapor bubbles. Fuel vapor bubbles are more dense than gas bubbles and will increase the local Weber number ($\mathrm{We} = \rho v^2 d/\gamma$) at the liquid-gas interface, which enhances breakup. Any effect seen with nitrogen bubbles will therefore be stronger with fuel vapor bubbles. It requires, however, that one can detect when cavitation bubbles form.

Investigations into bubble cavitation over the years [9,10,14–16] have shown that the generation and collapse of voids and bubbles generates pressure fluctuations in the surrounding medium. The primary breakup of the spray is furthermore dependent on cavitation, with the spray widths increasing with the size of the cavity [11]. Combining these methods with a technique to measure dispersion allows quantitative results on the influence of the presence of cavitation bubbles on the atomization process.

In this paper we combine investigations of sprays from glass and steel nozzles to study both the process within the nozzle and the breakup process at more relevant operating conditions. We also consider the dispersion and its relation with nozzle cavities.

In Sec. II, the effect of cavitation on the spray morphology is examined using transparent nozzles, high-speed DBI, and pressure measurements in the liquid supply line. In Sec. III, the contribution of cavitation to spray growth is investigated through dispersion measurements performed using laser-induced phosphorescence of lanthanide tracers [17–19] and linked to cavitation events through the measured pressure fluctuations.

## II. CAVITATION BUBBLES IN TRANSPARENT NOZZLES

To investigate the influence of cavitation in the nozzle on spray dispersion, both the internal nozzle flow and the resulting spray must be investigated at the same time. By using a fabricated glass nozzle in conjunction with a high-speed DBI technique, both internal and external flows can be visualized simultaneously. The experimental setup, shown in Fig. 1, uses a glass nozzle with a 200-$\mu$m capillary to produce a continuous water spray from a tank pressurized at 75 bars using $N_2$ gas. The internal dynamic nozzle pressure is measured using a flush-mounted dynamic pressure sensor (116A, PCB piezoelectronics), with a linear pressure response up to 80 kHz, sampled at a rate of 250 kHz to avoid aliasing. The pressure sensor output is amplified by a charge amplifier (Kistler, type 5011). A Photron SA-Z high-speed camera images the nozzle and spray simultaneously, illuminated by a high-power light-emitting diode (100 W, 6500 K). In order to visualize both the nozzle capillary and the spray onto the camera chip, a glass plate in front of the spray was used to equalize the optical object distances. The recorded images have a resolution of $1024 \times 144$ at a frame rate and exposure time of 120 kHz and 248 ns, respectively. The system has a magnification of 11.1 $\mu$m/pixel and a resolving power of 22.1 $\mu$m, measured using a USAF 1951 resolution chart. The start of the pressure measurement is synchronized to the camera through a Stanford DG535 pulse generator. By adding 0.1% by volume of Triton-X100 to the fluid, the surface tension of the fluid is significantly

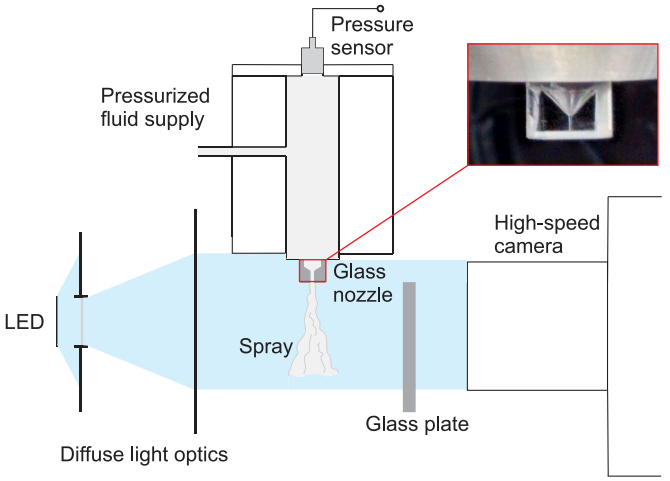


FIG. 1. Experimental setup used for the transparent nozzle measurements. A flush-mounted pressure sensor measures the dynamic fluid (water) pressure, while a high-speed camera images both the internal flow structures and the spray breakup at the same time.

reduced (from 70 to 30 mN/m) and large amounts of microbubbles are generated inside the flow. The reduced surface tension, similar to most fuels, will increase the instability of the surface of the jet and therefore enhance the breakup. However, this should not significantly affect a comparison between experiments with and without cavitation.

Figure 2 shows examples of the altered flows generated by differently sized bubbles. The bubbles deform into an elongated layer, expanded by the decrease in pressure along the nozzle capillary [20]. This is accompanied by an increased local velocity due to the decreased friction at the gas-liquid interface. The initial size of the bubble determines the size and duration of the cavitation bubble and has a large influence on the spray morphology, such as increases in spray width and enhanced atomization. The resulting cavitation bubble therefore has a large influence on the spray angle, as is reported in previous studies on cavitating nozzle flows [5,9,21]. See [22] for DBI recordings of bubbles with a diameter of 72 and 240 $\mu$m (regime III) bubbles passing through the glass nozzle and the resulting spray breakup. When a microbubble enters the nozzle, the pressure sensor records a pressure pulse, shown in Fig. 3(a). The pressure pulses are polluted by a frequency of 10 kHz, a resonance determined by the limitations of the charge amplifier. These pressure pulses occur at a fixed time [see Fig. 3(b)] before spray perturbation is observed, indicating that pressure measurements can also be used to identify the instant when a microbubble or cavity resides in the nozzle. In this way the effect of cavitation bubbles on the spray formation can be compared to the single-phase case under similar conditions, a unique opportunity relative to experimental conditions where a constant cavity is generated by extreme pressure differences over the nozzle capillary. These pressure pulses have an amplitude that increases with bubble size [see Fig. 4(b)], and therefore can be used as an indication of the size of the bubble and thus the size of the cavity.

It is important to note that the creation mechanism of this pressure wave is fundamentally different from the implosion of a collapsing cavitation bubble, which will likely result in larger absolute values of the pressure fluctuations. In this investigation the bubble is already present in the flow and a few mechanisms that likely contribute to the pressure pulse are the choking of the flow when the bubble enters the nozzle capillary, the separation of the gas layer into a collection of expanding and collapsing bubbles, and the release of the gas or vapor layer and the associated impact on the nozzle wall (as observed by Harrison [15]). In this investigation we focus on the first possibility.

In a simple model, the relation between the measured pressure pulse amplitude and the associated size of the bubble can be divided into three regimes (see also Fig. 5). In the first regime, the bubble

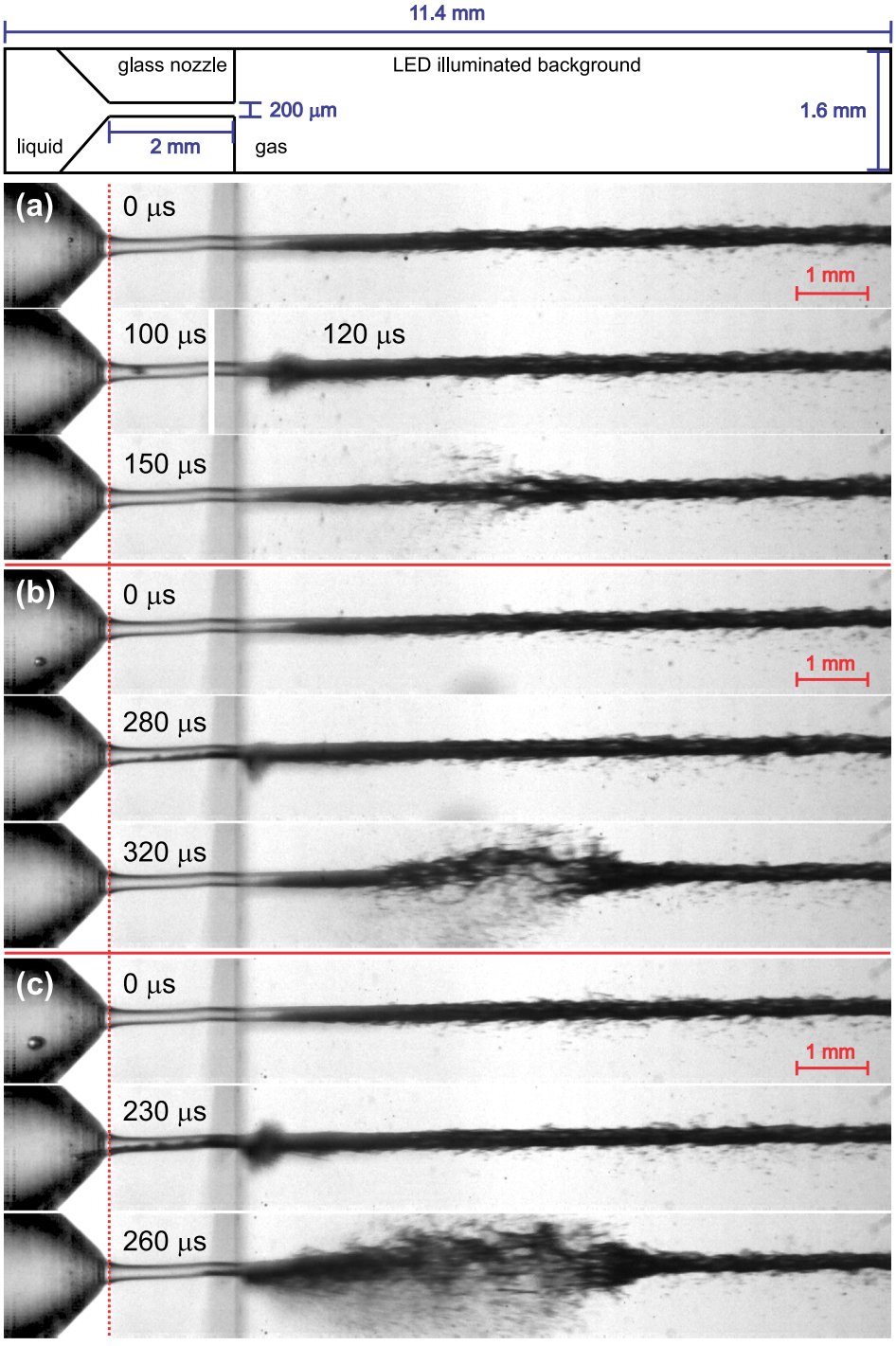


FIG. 2. Capillary cavities formed from the destruction (a) of 55-, (b) 100-, and (c) 190-$\mu$m bubbles and the resulting spray breakup. The region in front of the dotted red line has been enhanced in contrast and intensity to show the original size of the droplet. The middle image of (a) has been separated into two time steps to show both the traveling bubble and the emerging spray burst it creates. A collection of representative movies can be found in [22].

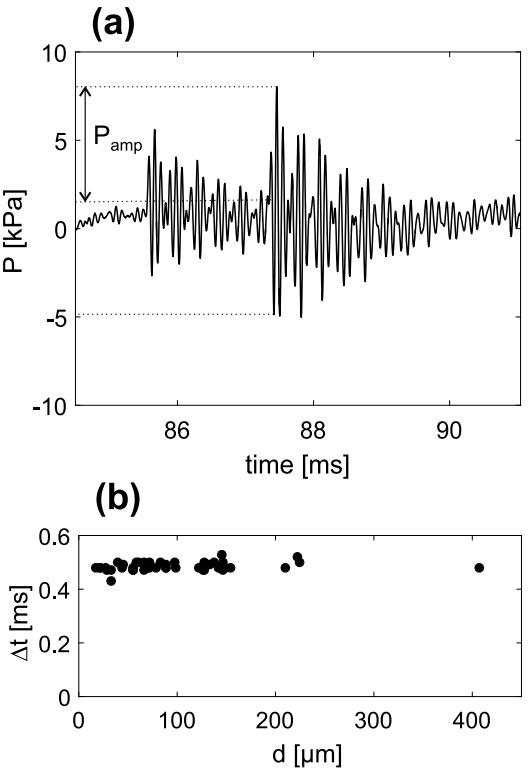


FIG. 3. (a) Pressure pulse amplitude associated with the cavity formation of Fig. 2(b). (b) The time delay $\Delta t$ between the first appearance of the emerging burst of fluid [see Fig. 2(b) at 280 $\mu$s] and the pressure pulse remains constant, independent of the bubble diameter.

diameter $d$ is small compared to the nozzle diameter $D$ ($d < D$) and the bubble does not deform upon entering the nozzle. The bubble forms a "plug" in the accelerating flow at the entrance of the capillary. The blocking bubble will cause a small pressure pulse, dependent on the change in mass flow. The pressure pulse amplitude that the bubble creates is therefore dependent on the change in mass flux through the nozzle. To determine the dependence of the changing mass flux on the size of the bubble, a standard Poiseuille velocity profile $v(r)$ is assumed, where $r$ is the distance from the center of the capillary, which using a cylindrical coordinate system (see Fig. 5, regime I) becomes

$$v(r) = \frac{\Delta P}{4\mu L}\left(\frac{1}{4}D^2 - r^2\right), \tag{1}$$

with $L$ the length of the nozzle, $\mu$ the dynamic viscosity of the fluid, and $\Delta P$ the pressure drop over the nozzle. The decrease in mass flow caused by the plug is due to the presence of the bubble. Assuming axisymmetry and a bubble placed at the center of the nozzle, the change in mass flow in terms of the bubble diameter $d$ can be described by

$$\Delta\dot{m} = \int_0^{D/2} \rho v(r) 2\pi r dr - \int_{d/2}^{D/2} \rho v(r) 2\pi r dr = \int_0^{d/2} \rho v(r) 2\pi r dr = \frac{\pi \Delta P}{128 \nu L} d^2(2D^2 - d^2), \tag{2}$$

with $\Delta\dot{m}$ the reduced mass flux through the nozzle entrance, $D$ the nozzle diameter, $\rho$ the density of the liquid, and $\nu$ its kinematic viscosity. This shows that for bubbles that do not deform upon entering the nozzle, the measured pressure amplitude has a dominant quadratic dependence on the

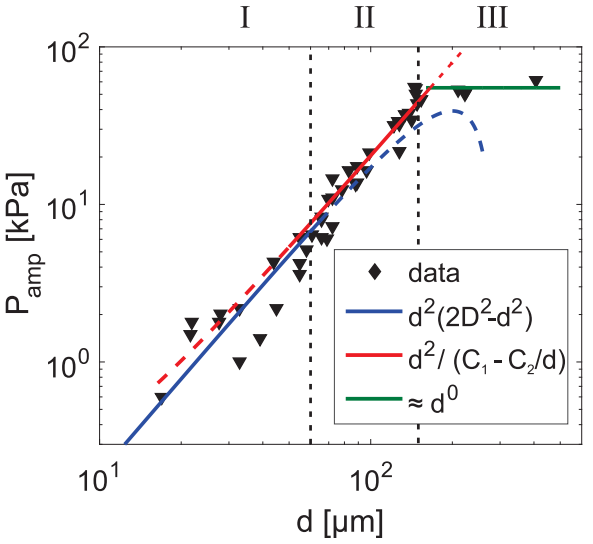


FIG. 4. The pressure pulse amplitude associated with each bubble diameter $d$ (the capillary diameter is denoted by $D$) shows a positive correlation between $P_{amp}$ and $d$. This can be divided into a plug regime (I), a developing regime (II), and a shear-dominated regime (III).

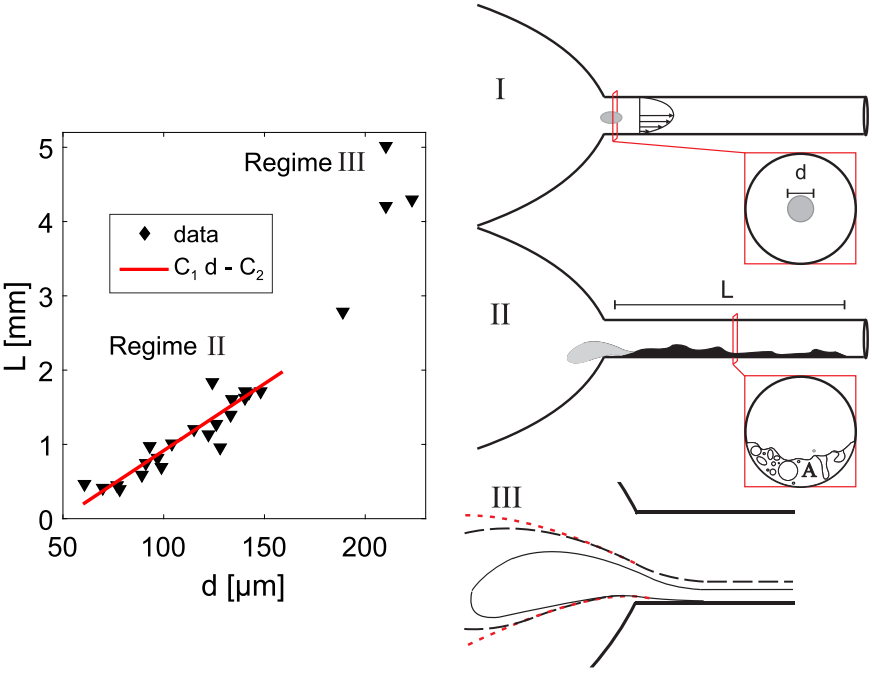


FIG. 5. Illustration of the generation of cavitation bubbles from seeded microbubbles. In the plug regime (I), the bubble forms a plug as it enters the nozzle and the alteration in mass flux causes the pressure pulse. In the developing regime (II) the bubble is deformed upon entrance and expands into a cavity. The cavity size or surface $A$ determines the changing mass flux and therefore $P_{amp}$. The cavity length $L$ is linearly dependent on the bubble size in this regime. In the shearing regime (III), the bubble is deformed by the accelerating fluid as it approaches the nozzle, forming into a cone shape. The position of the liquid-gas interface, and thus the size of $A$, no longer changes with increasing bubble size (red dotted line), merely deforming farther away from the nozzle capillary. As $A$ remains relatively constant in this regime, increases in $d$ significantly increase $L$.

measured bubble size [$P_{amp} \sim d^2(2D^2 - d^2)$]. For bubble diameters much smaller than the nozzle diameter ($d \ll D$) this reduces to a $d^2$ dependence. This model assumes a laminar flow, but a turbulent flow profile or flat velocity profile can be substituted and will merely change the prefactor, not the dominant $d^2$ dependence for small bubble diameters.

When the bubble size increases (above $d \approx 60$ $\mu$m in our case), the bubble does not enter the nozzle intact. It forms and expands into a cavity sheet, which grows towards the nozzle exit. Independent of the origin of the pressure pulse, the cross-sectional cavity area $A$ (see Fig. 5) determines the influence of the cavity formation on the pressure pulse; $A$ also determines the surface area of the choked flow. Moreover, together with the length of the sheet, it determines the size of the liquid-gas interface, i.e., the reduced friction as compared to the wall, and thus the acceleration of the fluid.

The deformation of the bubble into a sheet can be expressed as the formation of a cylindroid. The volume of a bubble will generate a sheet with a surface area $A$ and length $L$. Assuming $A$ can be approximated as $A = V_{bubble}/L$, the changing mass flux can be expressed as

$$\Delta\dot{m} = \rho v_n A = \frac{\rho v_n V_{bubble}}{L}, \tag{3}$$

with $v_n$ the velocity of the liquid inside the nozzle. Figure 5 shows that there is a linear relation between the bubble diameter and the cavity length $L = C_1 d - C_2$, with $C_1 = 18$ and $C_2 = 85$ $\mu$m. The relation between the mass flux change, i.e., the pressure pulse amplitude, and the bubble diameter then simplifies to $\Delta\dot{m} \sim \rho v_n d^3/L \sim \rho v_n d^3/(C_1 d - C_2) \sim \rho v_n d^2/(C_1 - C_2/d)$, which can be approximated as a $d^2$ relation for the sizes in regime II.

When the bubble size approaches the nozzle diameter, the bubble has more than enough volume to reach a quasisteady cavitating state. Because of its size, the bubble will be deformed into a cone shape while approaching the nozzle capillary, deformed by the shear of the accelerated fluid surrounding the bubble. In regime II, increases in bubble diameter lead to increases in $A$. However, in regime III, the surface area of the cavity at the capillary entrance no longer changes with the bubble size (see Fig. 5), as the bubble will merely start deforming further from the capillary entrance. This leads to significantly larger cavity lengths $L$, where larger bubble volumes deform into a sheet of nearly constant cross section. The area $A$, and thus the measured pressure pulse amplitude, becomes nearly independent of the bubble diameter (with an observed scaling of $P_{amp} \sim d^0$). A small dependence on the bubble diameter is likely to remain, but no significant evidence was found in this study for the available events.

This relation between internal pressure and cavity formation shows that cavitation events can also be predicted in nontransparent nozzles. The low wall roughness of glass nozzles, which increases jet stability (and decreases (delays) near-nozzle breakup), and relatively low injection pressure (to avoid structural failure) limit their physical relevance. To determine the effect of bubble cavities on the spray morphology of a more relevant nozzle type, material, and operating conditions, the glass nozzle in the setup of Fig. 1 is replaced by a stainless steel single-hole 200-$\mu$m nozzle. While the bubble size can no longer be determined inside this opaque nozzle, the effect of increased spray widths can still be determined. To quantify the width of a spray from DBI imaging, the full width at half maximum (FWHM) is recorded one nozzle diameter behind the exit (see Fig. 6). The ratio of spray widths $\theta$ between each time step (i.e., between successive frames), shown as $\theta_t/\theta_{t-1}$, is correlated to the accompanying pressure signal, shown in Fig. 7. The cloud of data points around zero pressure amplitude represents normal spray conditions, where no cavitation bubble event is detected. The increase in spray width shows in this particular measurement a linear correlation with the recorded pressure amplitude. This correlation suggests we are probing in regime I [see Fig. 4(b)] at small bubble sizes. However, the effect of capillary surface roughness on cavity generation, and therefore the generation of pressure waves, is unknown. Nonetheless, the data indicate that there is always a positive correlation between bubble size (spray width) and the amplitude of the measured pressure signal. The absolute values of this spray width increase will vary with the method of cavity generation and experimental conditions (ambient pressures, liquid properties, etc), but if a pressure pulse and a measurable increase in spray width are found to coincide, it is probable that cavitation-enhanced

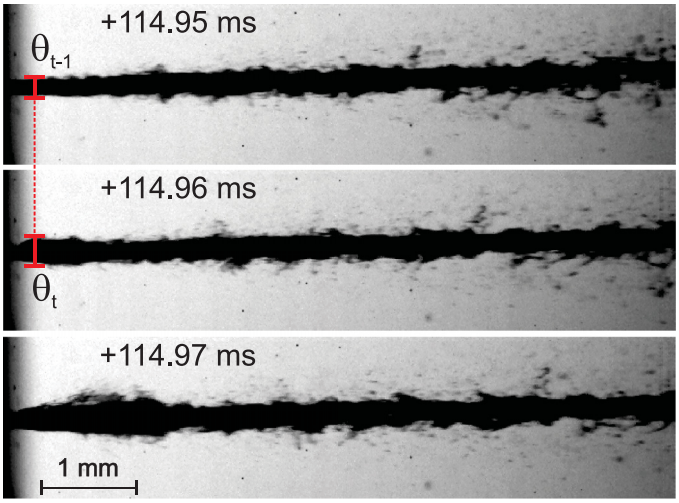


FIG. 6. Determination of the spray width ratio $\theta_t/\theta_{t-1}$ at three consecutive times through FWHM measurements one nozzle diameter downstream. The images, when compared to Fig. 2, also show the inherent differences in near-nozzle surface instability between the steel and glass nozzle sprays.

spray breakup is taking place. Using this relation, more quantitative measurement techniques can be used to determine the influence of cavity formation on the spray dispersion.

## III. SPRAY DISPERSION

Laser-induced phosphorescence tagging [18] is used to obtain quantitative measurements of spray dispersion. This technique uses ultraviolet (355-nm) laser pulses to excite ("tag") a small volume of fluid, which can subsequently be tracked by high-speed intensified cameras. Lanthanide-based

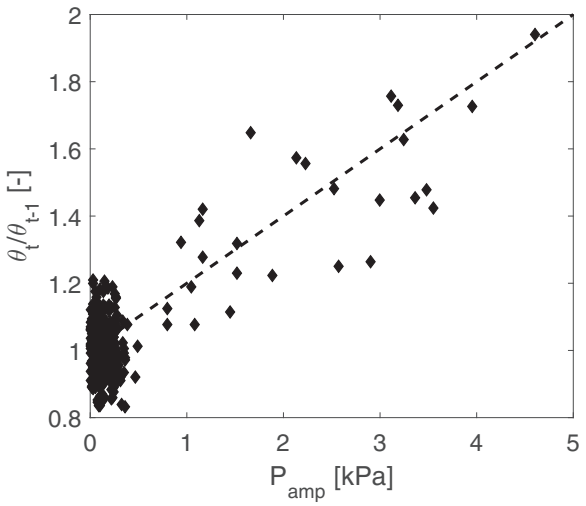


FIG. 7. Dependence of the spray width ratio, measured 200 $\mu$m after the nozzle exit, on the measured pressure pulse amplitude induced by cavitation bubbles. The dashed trend line emphasizes the strong correlation between the enhanced spray width and $P_{\text{amp}}$.

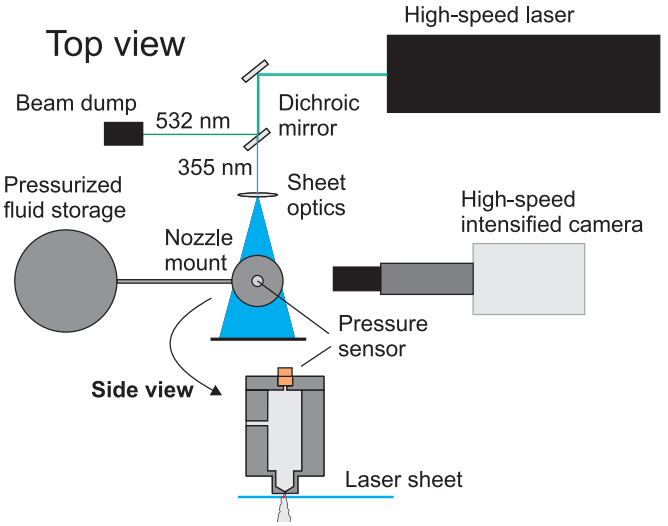


FIG. 8. Schematic view of the experimental setup used in the phosphorescence measurements. The camera, intensifier, pressure sensor, and laser are all synchronized with a trigger delay generator.

phosphorescence was shown in previous work [19] to have a large decay constant (≈800 $\mu$s in water-based sprays). Furthermore, the excitation energy required is minimal, a fluence on the order of ($\mu$J/cm$^2$)/pulse.

The setup of Fig. 1, using the steel nozzle, was altered for the phosphorescence measurements, as shown in Fig. 8. A standard 532-nm DM-20 high-speed laser (Photonics Ind.) was modified by inserting a DKDP type II third-harmonic crystal (Litron Lasers Ltd.) in the laser cavity to generate 150-ns pulses of 355-nm light at a repetition rate of 1 kHz with 30–40 $\mu$J/pulse. The UV light was focused into a thin sheet with an estimated fluence of 0.6–1 (mJ/cm$^2$)/pulse, passing immediately below the nozzle exit. The phosphorescence emission by the fluid was recorded at a frame rate of 100 kHz using a Photron SA-Z camera in combination with a HICATT GaAsP intensifier (Lambert instruments), with an exposure time of 300 ns to minimize motion blurring. The camera had a resolution of 1024 × 144 pixels, with a magnification of 17 $\mu$m/pixel. The intensifier quantum efficiency was ≈50% at the phosphorescence wavelength of 614 nm. The laser was synchronized with the camera and pressure sensor using a Stanford DG535 delay generator. The camera started imaging 3 $\mu$s after the laser pulse, to ensure that all fluorescence had died out. Approximately 60 000 individual phosphorescence sequences were measured, in which a total of 62 cavitation bubble events were found to coincide with the phosphorescence measurements, indicating the relative scarcity of cavitation bubble events.

Figure 9 shows an example of a phosphorescence sequence. The initially tagged fluid is seen to break up over time, forming ligaments and droplets due to Kelvin-Helmholtz instabilities. To determine the dispersion of the spray, the evolution of the deformation of the glowing fluid is tracked. By correlating radial or longitudinal profiles with previous frames (spatially stretched to account for possible deformations (dispersion)), the dispersion between successive time steps can be determined (for details see Ref. [18]). This processing method has an uncertainty of approximately 0.5% (±0.005 in the ratio of $\sigma_t/\sigma_{t-1}$), determined from synthetic images. As every sequence breaks up in a different way, caused by the unpredictable nature of the turbulent spray, the standard deviation associated with the dispersion is often fairly large [see Fig. 10(a)].

To identify the cavity-induced spray breakup sequences, both the initial width of the phosphorescent jet and the accompanying pressure signal are analyzed. If both show a strong increase, the sequence is analyzed for severe noise effects (hot pixels) that cause a failure in the

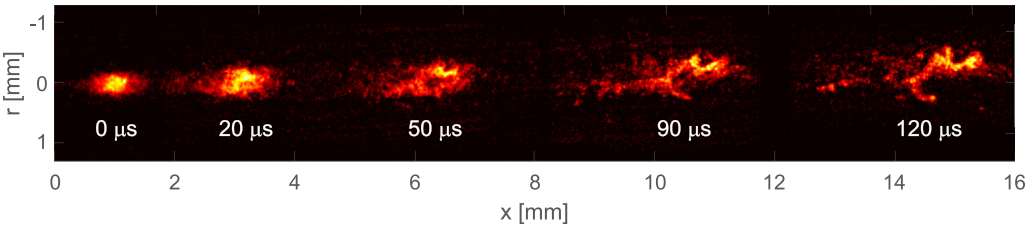


FIG. 9. Stills out of a single phosphorescence tagging sequence. An initially compact volume of fluid (≈10–20 nL), moving at ≈100 m/s, is tagged close to the nozzle exit. The dispersion can then directly be derived from the spread of glowing fluid.

width detection. If none are found, the average dispersion [of the $O(10^4)$ measurements without cavitation bubbles] is deducted from the sequence (see Fig. 10) and the resulting dispersion (growth rate) is averaged over all time steps to produce a single quantifier of the dispersion $\Pi$:

$$\Pi(i) = \frac{1}{t_{\text{end}} - t_0} \int_{t_0}^{t_{\text{end}}} \left( \frac{\sigma_t(i)}{\sigma_{t-1}(i)} - \left\langle \frac{\sigma_t}{\sigma_{t-1}} \right\rangle \right) dt, \tag{4}$$

where the average dispersion

$$\left\langle \frac{\sigma_t}{\sigma_{t-1}} \right\rangle = \frac{1}{N} \sum_{i=1}^{i=N} \left( \frac{\sigma_t(i)}{\sigma_{t-1}(i)} \right), \tag{5}$$

with $i$ the selected measurement sequence, $N$ the total amount of sequences in the measurement, $\sigma$ the width of the excited fluid in the radial or longitudinal direction, and $\sigma_t/\sigma_{t-1}$ the dispersion at time step $t$. This equation gives in one single number the increase (if $\Pi > 0$) or reduction ($\Pi < 0$) of the dispersion (growth rate) as compared to the average. Figures 11 and 12 show $\Pi$ in the radial and longitudinal directions, respectively, against the measured pressure pulse amplitude for each cavitation bubble. The standard deviation of approximately 5000 individual sequences is shown to indicate the variation in the dispersion in normal conditions. Unlike Figs. 4 and 7, Figs. 11 and 12

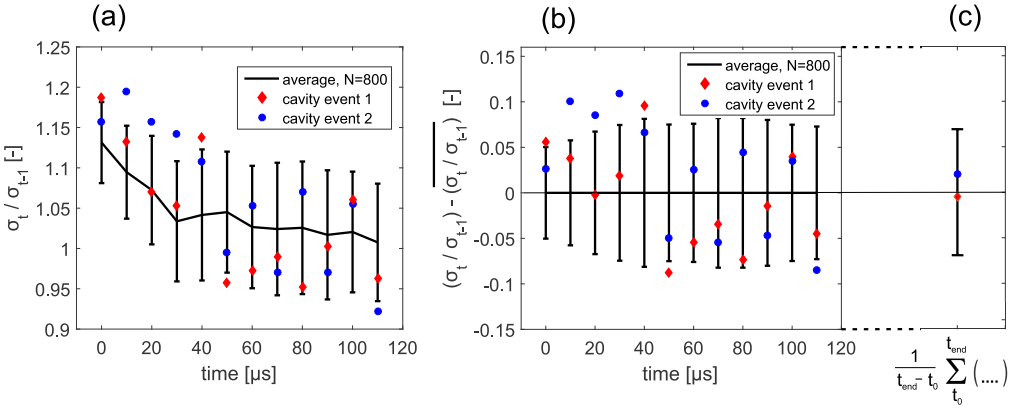


FIG. 10. (a) Radial dispersion (growth rate) measurement, in which the black line represents a mean of 800 sequences measured in one experiment. The two cavity events found in this experiment, determined from pressure measurements and spray width increases, are displayed as individual examples. (b) The average dispersion $\langle \frac{\sigma_t}{\sigma_{t-1}} \rangle = \frac{1}{N} \sum_{i=1}^{i=800} (\frac{\sigma_t(i)}{\sigma_{t-1}(i)})$ is deducted from the measurement and (c) the cavity events are time averaged. This shows the time-averaged dispersion of both cavity events as compared to normal conditions, represented by the standard deviation.

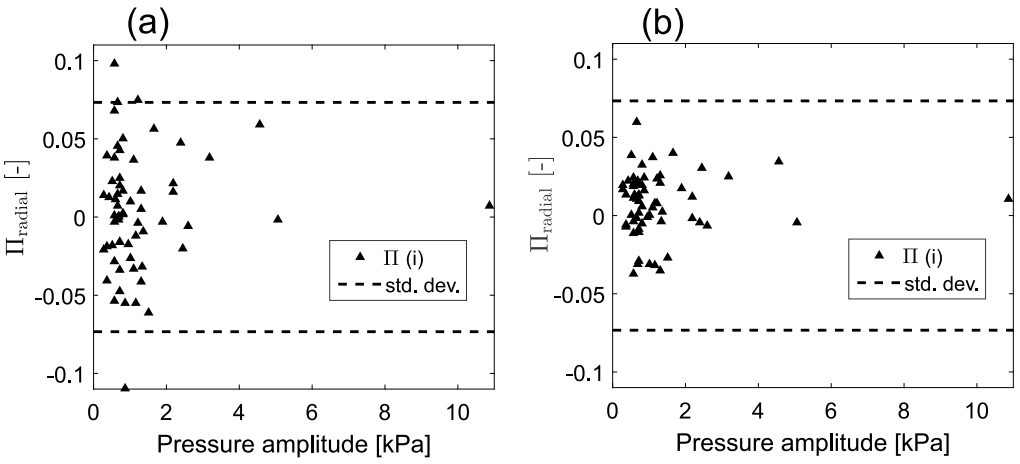


FIG. 11. Comparison of the radial dispersion difference Π of the accumulated cavity events $i$, averaged over (a) 30 $\mu$s and (b) 120 $\mu$s, compared to the standard deviation (indicated by the dashed horizontal lines) of the spray dispersion during normal conditions.

show no discernible correlation with the measured pressure pulse amplitude, i.e., the cavity size. Even when the number of time steps in the computation of Eq. (4) is decreased, i.e., looking closer to the nozzle exit, it only increases the spread of the dispersion difference. This is in contrast to the result in Fig. 7, which shows a clear increase in spray width (angle) over a smaller range of pressure amplitudes. It should be noted that the events shown in Figs. 11 and 12 are all of bubble sizes in regimes I and II. The natural skewness in the bubble distribution towards smaller bubbles, together with the small probe volume required in laser-induced phosphorescence, creates a relative scarcity in the dispersion measurements. Bubbles in regime III, which occur at a rate of only $\approx 2/\text{s}$, were not found in the investigated 60 000 measurements (corresponding to approximately 192 ms total measurement time). However, from Fig. 7 we can see that even in regimes I and II, a strong correlation between the pressure pulse amplitude and the qualitative spray width (angle) exists and should be visible in the available measurements.

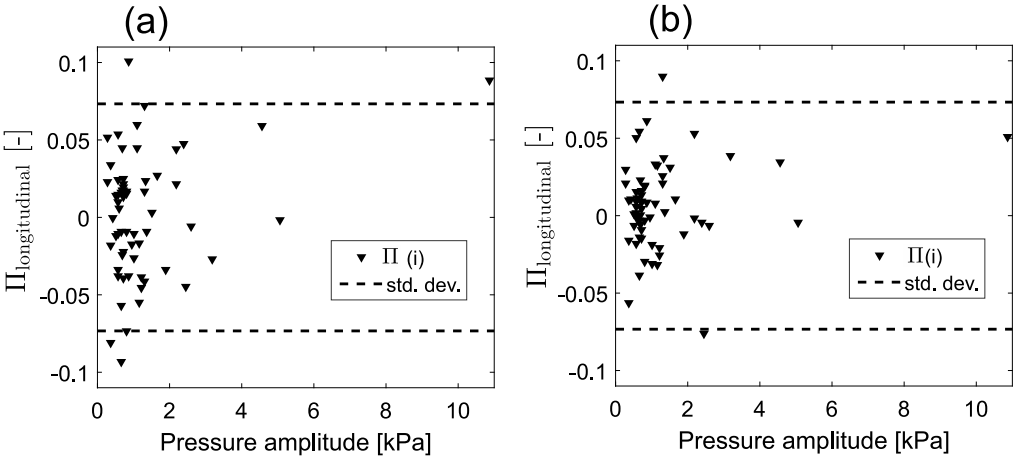


FIG. 12. Comparison of the longitudinal dispersion difference Π of the accumulated cavity events $i$, averaged over (a) 30 $\mu$s and (b) 120 $\mu$s, compared to the standard deviation (indicated by the dashed horizontal lines) of the spray dispersion during normal conditions.

The results discussed in this section indicate that the dispersion (growth rate) caused by primary breakup is not enhanced by cavitation events. The mass flow, spray width (angle), and atomization will be enhanced by the formation of cavities. However, the dispersion, which turns out to be independent of the starting width of the excited fluid, remains unchanged. This indicates that the shear-induced turbulence, in both the liquid and gas phases, that generates dispersion is not significantly affected by the starting width of the spray.

## IV. CONCLUSION

Cavitation bubble formation in the nozzle capillary is investigated through high-speed imaging of a transparent nozzle, simultaneously recording the dynamic fluid pressure inside the mount. It is found that, in regimes II and III, the bubbles deform and expand into a sheet by the strongly converging flow, mimicking a transient cavity inside the capillary. The recorded pressure pulse amplitudes scale with the size of the bubble in regimes I and II, as the diameter determines the size and length of the formed cavity.

The bubble-induced cavities are found to increase the spray width and to be related in a similar fashion to the pressure-pulse amplitude. By monitoring the internal pressure it is therefore possible to predict the formation of a cavitation bubble without the use of a transparent nozzle or x-ray imaging.

The dispersion of tagged spray volumes has been measured using laser-induced phosphorescence, synchronized with measurements of nozzle pressure. The dispersion measured during a bubble cavity formation event is compared to the average measurements and no significant increase was found. This suggests that while a cavity may increase the mass flow and spray widths and may decrease droplet size, the dispersion of the spray is not significantly affected. The shear-induced turbulence that determines the dispersion, both primary breakup and the spray-induced gas-phase turbulence, is not dependent on the amount of fluid (mass flow) leaving the nozzle or on the spray angle.

## ACKNOWLEDGMENTS

We thank Michel Versluis for his helpful comments on this work. This work is part of the research programme DROP of the Foundation for Fundamental Research on Matter (FOM), which is part of the Dutch Organisation for Scientific Research (NWO).

[1] L. P. Bayvel and Z. Orzechowski, *Liquid Atomization* (Taylor and Francis, London, 1993).
[2] J. Dec, A conceptual model of DI diesel combustion based on laser-sheet imaging, SAE Report No. 970873, 1997.
[3] A. H. Lefebvre, *Atomization and Sprays* (Taylor and Francis, London, 1989).
[4] K. Masters, *Spray Drying Handbook* (Longman Scientific and Technical, Harlow, 1991).
[5] J. M. Desantes, R. Payri, F. J. Salvador, and J. De la Morena, Influence of cavitation phenomenon on primary break-up and spray behavior at stationary conditions, Fuel **89**, 3033 (2010).
[6] L. C. Ganippa, G. Bark, S. Andersson, and J. Chomiak, Comparison of cavitation phenomena in transparent scaled-up single-hole diesel nozzles, *CAV 2001: Fourth International Symposium on Cavitation*, Pasadena, 2001.
[7] N. Mitroglou, M. Gavaises, J. Nouri, and C. Arcoumanis, Cavitation inside enlarged and real-size fully transparent injector nozzles and its effect on near nozzle spray formation, *Droplet Impact Phenomena and Spray Investigations Workshop*, Bergamo, 2011.
[8] H. K. Suh and C. S. Lee, Effect of cavitation in nozzle orifice on the diesel fuel atomization characteristics, Int. J. Heat Fluid Flow **29**, 1001 (2008).
[9] A. Sou, S. Hosokawa, and A. Tomiyama, Effects of cavitation in a nozzle on liquid jet atomization, Int. J. Heat Mass Transfer **50**, 3575 (2007).

[10] C. Mauger, L. Mees, M. Michard, A. Azouzi, and S. Valette, Observations of the dynamics and acoustics of traveling bubble cavitation, Exp. Fluids **53**, 1895 (2012).
[11] M. Michard, C. Mauger, and L. Mees, Etude de la cavitation dans une buse d'injection transparente, *Proceedings of the 13th Congres Francophone de Techniques Laser* (CORIA, Rouen, 2012).
[12] D. J. Duke, A. L. Kastengren, F. Z. Tilocco, A. B. Swantek, and C. F. Powell, X-ray radiography measurements of cavitating nozzle flow, Atomization Sprays **23**, 841 (2013).
[13] D. J. Duke, A. Swantek, A. L. Kastengren, K. Fezzaa, and C. F. Powell, Recent developments in x-ray diagnostics for cavitation, SAE Int. J. Fuel Lubricants **8**, 135 (2015).
[14] S. L. Ceccio and C. E. Brennen, Observations of the dynamics and acoustics of travelling bubble cavitation, J. Fluid Mech. **233**, 633 (1991).
[15] M. Harrison, An experimental study of single bubble cavitation noise, J. Acoust. Soc. Am. **24**, 776 (1952).
[16] G. E. Reisman, Y. C. Wang, and C. E. Brennen, Observations of shock waves in cloud cavitation, J. Fluid Mech. **355**, 255 (1998).
[17] N. Arnaud and J. Georges, Comprehensive study of the luminescent properties and lifetimes of $Eu^{3+}$ and $Tb^{3+}$ chelated with various ligands in aqueous solutions: Influence of the synergic agent, the surfactant and the energy level of the ligand triplet, Spectrochim. Acta A **59**, 1829 (2003).
[18] D. D. van der Voort, B. C. S. de Ruijter, W. van de Water, N. J. Dam, H. J. H Clercx, and G. J. F. van Heijst, Phosphorescent flow tracking for quantitative measurements of liquid spray dispersion, Atomization Sprays **26**, 219 (2016).
[19] D. D. van der Voort, N. C. J. Maes, T. Lamberts, W. van de Water, R. P. J. Kunnen, H. J. H Clercx, G. J. F. van Heijst, and N. J. Dam, Lanthanide-based laser-induced phosphorescence for spray diagnostics, Rev. Sci. Instrum. **87**, 033702 (2016).
[20] M. S. Plesset and A. Presperetti, Bubble dynamics and cavitation, Annu. Rev. Fluid Mech. **9**, 145 (1977).
[21] R. Payri, F. J. Salvador, J. Gimeno, and J. de la Morena, Study of cavitation phenomena based on a technique for visualizing bubbles in a liquid pressurized chamber, Int. J. Heat Fluid Flow **30**, 768 (2009).
[22] See Supplemental Material at http://link.aps.org/supplemental/10.1103/PhysRevFluids.2.033601 for DBI recordings of 72-$\mu$m-diam (regime II) and 240-$\mu$m-diam (regime III) bubbles passing through the glass nozzle and the resulting spray breakup.